Reversible and nonvolatile tuning of photoluminescence response by electric field for reconfigurable luminescent memory devices

Ming Zheng[*], Hai Ling Sun, Man Kit Chan, and Kin Wing Kwok[*]

Department of Applied Physics, The Hong Kong Polytechnic University, Kowloon, Hong Kong

Abstract

Luminescent materials with reversibly tunable ability under external stimuli, e.g., strain and electric field, are of great interest for developing advanced multifunctional optical devices. An important problem that has not been solved is the nonvolatility of field-driven switching for information storage applications. Here, we first propose a design principle that the electrically induced ferroelastic domain engineering in $0.7Pb(Mg_{1/3}Nb_{2/3})O_3$-$0.3PbTiO_3$ substrates can be used to achieve robust nonvolatile tuning of photoluminescence performance in elastically-coupled Pr-doped $Ba_{0.85}Ca_{0.15}Ti_{0.9}Zr_{0.1}O_3$ thin films in a reversible way. Such a nonvolatile and reversible response is striking, which stems from the intermediate lateral-polarization-induced stable strain state in the substrate during domain switching. The quantitative determination of strain-mediated photoluminescence intensity is also addressed by virtue of the converse piezoelectric effect. This study points to an effective strategy for realizing piezo-luminescent effect in ferroelectric thin-film heterostructures and demonstrates great potentials in designing reconfigurable, low-power nonvolatile luminescent memory devices.

Keywords: PMN-PT; photoluminescence; nonvolatile; reversible; ferroelastic strain

---

[*] Corresponding authors. *E-mail addresses*: zhengm@mail.ustc.edu.cn (M. Zheng), apkwkwok@polyu.edu.hk (K.W. Kwok).

Introduction

The photoluminescence (PL) properties of lanthanide ions have attracted continuing interest because of their promising applications in laser mediums, display lighting, biological assaying, and medical imaging, etc [1-6]. *In situ* rapid and reversible modulation of the PL activity using external stimuli, e.g., strain, magnetic and electric fields [7-13], draws growing popular attention and has been realized in rare-earth-doped ferroelectric bulk ceramics and thin films [8-13]. One of the methods is to integrate ferroelectric film hosts with highly piezoelectric $Pb(Mg_{1/3}Nb_{2/3})O_3$-$PbTiO_3$ (PMN-PT) wafers and then modify the PL properties of thin films using linear piezo response of the PMN-PT [11-13]. However, the piezostrain recovers to the original value after turning off the driven field, and thus the tuning of PL is volatile. From the perspective of the memory device application, it is highly desirable to control PL properties in a nonvolatile manner around the ambient temperature. In many well-known nonvolatile memories such as ferroelectric random access memory (FeRAM), magnetic random access memory (MRAM), and resistive switching random access memory (RRAM), etc., the binary information is often generated by three quantities, i.e., the direction of polarization, the direction of magnetization, and the value of resistance. Here, we prove that an alternative quantity-the level of the PL intensity-can be exploited to store digital information efficiently. The challenge in nonvolatile tuning is how to maintain the produced status upon the external field has been switched off. Recently, a breakthrough has been reported [14,15] that besides the dual stable upward ($+P$) and downward ($-P$) remnant polarization states, there also exists an metastable state during polarization switching in the PMN-PT

crystals, where most of polarization vectors lie in the lateral direction. Therefore, two kinds of reversible and nonvolatile residual strains can be obtained through rotating the ferroelectric domains between the longitudinal (upward or downward) and lateral directions by imposing proper external fields (i.e., domain-engineered ferroelastic switching) [14,15], which offers the possibility of nonvolatile switching of multiple functionalities. Based on this principle, the nonvolatile modulation of physical properties has been demonstrated in several functional thin films, including ferromagnetic alloy [16-18], ferrimagnetic ferrites [19], vanadium oxides [20], ruthenium oxides [21], and colossal magnetoresistive manganites [22-25], through ferroelastic strain effect. In spite of those efforts dedicated to *in situ* reversible modulation of lattice-sensitive PL response for rare-earth-doped ferroelectric oxide films by piezostrain, nonvolatile control of PL properties for luminescent memory devices by electric field is still missing. Moreover, most nonvolatile lattice strain effects on physical properties are focused on (001)- and (011)-oriented PMN-PT single crystalline substrates. The report on (111)-oriented PMN-PT as substrate and the nonvolatile control of PL properties is limited.

Motivated by this, we have studied the electric field effect on the PL response of Pr-doped $Ba_{0.85}Ca_{0.15}Ti_{0.9}Zr_{0.1}O_3$ [$(Ba_{0.85}Ca_{0.15})_{1-x}Pr_xTi_{0.9}Zr_{0.1}O_3$, abbreviated as BCTZ:Pr] thin films by depositing them onto the PMN-PT single crystals with $La_{0.7}Sr_{0.3}MnO_3$ (LSMO) as the buffered electrode. The host of BCTZ here is among the most extensively studied lead-free ferroelectrics recently because of its excellent piezoelectricity (d_{33}~620 pC/N) [26]. Lanthanide Pr^{3+} ion is chosen as dopant in the BCTZ host since its PL mission intensity is dependent on the $4f5d$ configuration level, which is highly sensitive

to the structural symmetry of BCTZ host [9,27]. Here, we doped 0.2 mol% Pr in BCTZ host to obtain the optimal PL signal [28]. Our findings demonstrate the validity of the conjecture that two stable and nonvolatile PL responses can be produced at room temperature by taking advantage of the reversible ferroelastic strain effect of the substrate. Further, we also found that the PL intensity increases linearly with the piezostrain. This work opens a door for developing thin film based future luminescent prototype devices for information storage applications.

Experimental section

Thin film growth

Both the LSMO buffered electrodes and the BCTZ:Pr films were fabricated on (111)- and (001)-cut PMN-PT commercial single crystalline wafers via the pulsed laser deposition (PLD) technique. Two targets were ablated at 700 °C in pure oxygen of 20 and 25 Pa for the LSMO and BCTZ:Pr films, respectively. Subsequently, both the films were post-annealed under pure oxygen of 1000 Pa for 30 minutes to eliminate oxygen vacancies. The thicknesses of the LSMO and BCTZ:Pr layers are 40 and 200 nm, respectively.

Structural, lattice strain, and PL characterization

The film structure was analyzed using a four-circle X-ray diffractometer (XRD, SmartLab, Rigaku Co., Japan) attached with Cu $K_{\alpha 1}$ (λ=1.5406 Å) radiation. The PL data were collected via an Edinburgh FLSP920 spectrophotometer. Due to the much huger resistance (~10^9 Ω) of the PMN-PT substrate than that (~10^3 Ω) of the LSMO film, the conductive LSMO film actually serves as the top electrode in the LSMO/PMN-PT/Ag

structure. The polarization of the PMN-PT was conducted by vertically imposing voltages using a Keithley 2410 sourcemeter across the structure through the conductive LSMO top electrode and the sputtered bottom silver (300 nm) electrode. Note that the LSMO top electrode was always kept at ground when imposing the poling fields. Figure 1a and b illustrate the electric field configuration for measurements of PL response and longitudinal strain of the structures, respectively. The arrows indicate the polarization direction of the PMN-PT. The electrically induced lateral strain of the PMN-PT was recorded by strain gauge (Figure 2d). Prior to any measurement, we applied a large field (e.g., E=+10 kV/cm) to the structures for about 30 minutes to guarantee that the substrate is fully positively poled [i.e., the polarization vectors point to the LSMO film denoted by P_r^+ in Figure 2b]. All the measurements were conducted in the ambient temperature condition.

Results and discussions

Figure 1c and e show the XRD linear θ-2θ scan patterns of the BCTZ:Pr thin films deposited on the LSMO-coated PMN-PT(111) and PMN-PT(001), respectively. Only (lll) (l=1, 2) and (00l) (l=1, 2, 3) reflections from the LSMO and the PMN-PT appear, revealing the single phased nature of LSMO films with perovskite structure. To inspect the in-plane crystallographic orientation of the film, XRD ϕ-scans were performed on the (101) reflection peaks of the LSMO and the substrate (insets of Figure 1c and e). As depicted in Figure 1d and f, two sets of trifold (fourfold) reflection peaks 120° (90°) apart from each other were found from the LSMO and the substrate, respectively, which clearly suggests good epitaxial feature of the LSMO on the substrate. Note that for the

LSMO/PMN-PT(111) structure, both the LSMO and the PMN-PT contain a fraction of 60° rotated grains in the (111) plane, as reflected by another three weaker reflection peaks. In addition, the reflection peak of the BCTZ:Pr film was hard to distinguish from that of the PMN-PT because of their quite close lattice parameters. Only the (lll) or (00l) peaks of BCTZ:Pr arise along with those of the PMN-PT and the LSMO. This implies that both the BCTZ:Pr films were deposited on LSMO-buffered PMN-PT crystals in an epitaxial way, which makes it possible to obtain strong elastic coupling at the interfaces of the structures.

In order to explore ferroelastic control of BCTZ:Pr films on PMN-PT, the lateral strain [$\delta\varepsilon_{xx(PMN\text{-}PT)}$] of the PMN-PT(111) was first studied against electric field as measured using strain gauge [see Figure 2d]. When imposing a large field (e.g., E=9 kV/cm>$E_{C(PMN\text{-}PT)}$) presented in Figure 2a, a symmetrical butterfly-like strain curve (green) was observed owing to 180° polarization reorientation. Nevertheless, upon cycling a suitable small field (e.g., E=2 kV/cm<$E_{C(PMN\text{-}PT)}$), we found a hysteretic response (red) of in-plane strain to E, arising from non-180° ferroelastic polarization switching [14,15]. Apart from the initial strain state (**O** state), an electric-field-induced lateral tensile strain state (**B** state) can also be achievable due to the stable residual lateral polarization vectors in the PMN-PT(111) (denoted by $P_r^{//}$ in Figure 2c) [14,15]. Such two stable, switchable, and nonvolatile residual strain states (**O** and **B**) have been utilized to realize stable, reversible, and nonvolatile tuning of different types of lattice-coupled physical properties, such as ferromagnetic resonance frequency [18], metal-insulator transition temperature [20], room-temperature resistance [21,22], magnetoresistance

6

effect [23,24], and photoresistance effect [25], etc., in various PMN-PT based systems. Hence, we anticipate that this unique ferroelastic domain engineering, in conjunction with the strong mechanical coupling across the interfaces of the BCTZ:Pr/LSMO/PMN-PT epitaxial structures, will make the system amenable to electric-field-controlled nonvolatile manipulation of PL performance by adjusting the voltage in close proximity to the $E_{C(PMN-PT)}$.

Figure 3a depicts the PL emission spectra of the BCTZ:Pr(111) film when the PMN-PT(111) substrate was under the longitudinal (P_r^+) and lateral ($P_r^{//}$) polarization directions, respectively. Similar to other PL materials doped by Pr [9,28,29], the BCTZ:Pr film gave a very good PL signal of Pr^{3+}. The emissions centered at 544, 578, 610, 627, and 647 nm correspond to $^3P_0 \rightarrow {}^3H_5$, $^3P_1 \rightarrow {}^3H_6$, $^1D_2 \rightarrow {}^3H_4$, $^3P_0 \rightarrow {}^3H_6$, and $^3P_0 \rightarrow {}^3F_2$ transitions of Pr^{3+} ions, respectively. Accompanied by the polarization vectors switched from the P_r^+ to the $P_r^{//}$ state, the PL intensity of the BCTZ:Pr was reduced visibly, especially for the strong green (at 544 nm) and red (at 610 nm) emission peaks. Previous experiments have confirmed that the PL emission strongly correlates with the crystallographic symmetry of the host and the induced different crystal field strengths near the lanthanide ions according to the Judd-Ofelt (J-O) theory [30,31]. A higher-symmetric host would generate a crystal field incorporating less uneven components near Pr^{3+}, which decreases the 4f-4f electric dipolar transition probabilities of Pr^{3+} [32,33]. Namely, the higher structural symmetry, the weaker PL emission. Consequently, we carried out XRD linear scans to probe the structural variation of the BCTZ:Pr/LSMO/PMN-PT heterostructure. As seen in Figure 3b, both of the (111)

reflection peaks of the PMN-PT and the LSMO gradually move to higher angles after the polarization rotated from the P_r^+ to the $P_r^{//}$ state, disclosing a longitudinal contraction associated with an effective lateral expansion of both the substrate and the film. The electrically induced lateral tensile strain of the PMN-PT can be migrated into the BCTZ:Pr through the LSMO layer, leading to smaller tetragonal distortion of the BCTZ:Pr film. Therefore, the electrically controlled PL response can be ascribed to strain-mediated higher symmetry of the host, which reduces radiative transition probabilities of the dopant ions.

On the basis of this electric tunable ferroelastic strain effect, we proved the feasibility of a low-power luminescent information storage cell. As illustrated in Figure 4a, the reversible and nonvolatile PL states were generated by imposing voltage pulses with the amplitude of E=-2 kV/cm for the "ON" state and E=+2 kV/cm for the "OFF" state, respectively. Such a ferroelastic control of PL switching in a reversible and nonvolatile manner can be qualitatively understood using the illustrations in Figure 4b and c. Prior to the measurement after imposing a large positive field E=+10 kV/cm, the substrate is absolutely positively polarized and its polarization vectors only point to r1$^+$ (i.e., P_r^+ state) (see Figure 4b). Then upon imposing a small negative E=-2 kV/cm [|E| close to but lower than $E_{C(PMN-PT)}$] to the positively poled substrate, the PMN-PT(111) is partially depolarized. The polarization undergoes 71° and 109° ferroelastic switching from r1$^+$ to r2$^+$/r3$^-$/r4$^+$ and from r1$^+$ to r2$^-$/r3$^+$/r4$^-$, respectively, which results in the polarization rotated from the longitudinal to the lateral direction (i.e., $P_r^{//}$ state) (see Figure 4c). This domain switching gives rise to a lateral tensile strain in the PMN-PT,

corresponding to the strain change from *O* to *A* state in Figure 2a. After the field *E*=-2 kV/cm is switched off, the lateral strain evolves from *A* to *B* rather than to *O* state because of stable residual lateral polarization state of the PMN-PT(111). The generated residual lateral tensile strain was diverted into the BCTZ:Pr through the LSMO layer, which lowers the tetragonal distortion of the host and suppresses the PL emission of the film. Afterwards, the polarization vectors were rotated from the lateral (*B* state) to the longitudinal (*C* state) direction by imposing *E*=+2 kV/cm, releasing the previously introduced residual lateral tensile strain. If removing the *E*=+2 kV/cm, the lateral strain recovers to its virgin value. As a result, the PL intensity of the film also returns to its original state. Prior to the voltage cycling measurement, we applied a positive field pulse for several times at an interval of 50 s to verify that the PL state can be read out stably, as shown in Figure 4a. The PL switching of our structure also shows excellent retention properties (not shown here), which is favorable for memory device application. In our previous paper [22-25, 34], binary stable resistance states can be stored by imposing a sequence of electric field pulses. In this work, the principle of using the PL intensity instead of commonly used resistance state to store digital information opens a significant avenue towards developing future memory devices. Compared with the multilevel resistance states in RRAM by controlling light or moisture [35,36], the multiple levels of the PL emission intensity can be used to double confirm the storage information because the emission includes different wavelengths (e.g., 544 or 610 nm). Moreover, the writing operation is rapid and energy efficient by imposing an electric field pulse, not like that in conventional flash memory. In addition, the reading operation becomes easy instead of

the destructive reading of polarization in FeRAM and the complicate detect of local magnetization in MRAM. Notably, if the amplitude of applied negative field rises from |E=-2 kV/cm| to |E=-3 kV/cm|, larger than $E_{C(PMN-PT)}$, the PL intensity will be enhanced, leading to smaller tunability of PL emission. The difference between these two PL responses for pulse fields E=-3 and -2 kV/cm arises from the conversion of a fraction of polarization vectors from the lateral to the longitudinal direction, which produces diverse residual strain states. This result discloses the importance of choosing suitable amplitude of pulse electric field in maximizing the ferroelastic strain, and thus achieving greater nonvolatile modulation of PL response.

To further substantiate the quantitative correlation between the PL and the strain, we manipulated the *in situ* PL intensity using the linear piezo response without domain switching. The electrically induced relative variation of the PL intensity ($\Delta I/I$) was plotted against electric field applied to the PMN-PT(001) in Figure 5a. Here, the PMN-PT(001) crystal is selected instead of the PMN-PT(111) one owing to its larger piezoelectric coefficient (d_{33}>2000 pC/N). With increasing field from E=0 to 10 kV/cm, both the PL responses for the strong green (at 544 nm) and red (at 610 nm) emission peaks are gradually reinforced. For example, the intensity increases by 5.3% and 6.6% for the green and red peaks, respectively. As shown in Figure 5b, both the PL intensities show a linear dependence on E, caused by the linear lateral lattice contraction of the PMN-PT originating from its converse piezoelectric effect (see inset of Figure 5b) [23,37]. Thus, $\Delta I/I$ can be written as $\Delta I/I=aE$. *In situ* XRD measurements in Figure 5c indeed reveal that both of the (002) peaks of the PMN-PT and the LSMO move to lower

Bragg angles with increasing E, which means that both the lattice parameters c of the PMN-PT and the LSMO are expanded. As shown in the inset of Figure 5c, the relative evolution of the lattice parameter c [$\delta\varepsilon_{zz(PMN-PT)}$] of the PMN-PT exhibits a linear response to E, implying the piezoelectric feature of the produced strain in the substrate. This linear strain was diverted into the LSMO and further to the BCTZ:Pr film, leading to a linear dependence of $\delta\varepsilon_{zz(LSMO)}$ and $\delta\varepsilon_{zz(BCTZ:Pr)}$ on E. The relationship between $\delta\varepsilon_{zz(BCTZ:Pr)}$ and E could be expressed as $\delta\varepsilon_{zz(BCTZ:Pr)}=bE$. Using the Poisson relation $\delta\varepsilon_{zz}=-2v/(1-v)\delta\varepsilon_{xx}$ [38], the quantitative determination of the $\Delta I/I$ and the lateral strain of the BCTZ:Pr film can be described as $\Delta I/I=(a/b)[-2v/(1-v)]\delta\varepsilon_{xx(BCTZ:Pr)}$. Here, v is the Poisson ratio. Actually, we observed a linear response of the $\Delta I/I$ of the film to the produced lateral strain of the substrate, as shown in Figure 5d. The PL intensity-strain relationship indicates that the relative variation of PL intensity in the BCTZ:Pr is directly proportional to its generated lateral compressed strain. By combining PL and XRD measurements and considering the small screening length (~nm) of the electron in LSMO film, it is reasonable to exclude the electrostatic charge-mediated PL change in our structure. This finding explicitly establishes the effectiveness of strain control of PL performance of lanthanide emitter ions by imposing appropriate electric fields.

Although we have verified the feasibility of electrically induced nonvolatile tuning of the PL response of the BCTZ:Pr films by exploiting the ferroelastic domain engineering of the PMN-PT, we also expect a similar tuning to be possible if lanthanide emitter ions are hosted in other lead-free BaTiO$_3$ [12,13], Bi$_{0.5}$Na$_{0.5}$TiO$_3$ [4,10], and K$_{0.5}$Na$_{0.5}$NbO$_3$ [33,39] based perovskite oxide films on the PMN-PT. Particularly, in the

recent past the electric-field-controlled strain-mediated single-domain ferromagnetic state, spin manipulation, and magnetic uniaxial anisotropy have been reported in several metal nanostructures elastically coupled to the PMN-PT, such as nickel nanocrystals [40], nanoislands [41], and nanosquares [42]. Remarkable strain induced by electric field is also possible to be transferred to rare-earth-doped $NaYF_4$ based nanocrystals [3,7] by depositing them onto the PMN-PT, and such systems are also potential candidates for electrically driven nonvolatile switching of PL performance.

Conclusions

In summary, we report an electric-field-induced nonvolatile and reversible tuning of PL response using well-designed BCTZ:Pr/LSMO/PMN-PT epitaxial heterostructures. We attribute this to two dissimilar stable, reversible and nonvolatile strain states produced by using an exotic ferroelastic domain switching pathway in the PMN-PT(111), which can adjust the crystallographic symmetry of the BCTZ films and thus the local crystal field strength near the Pr^{3+}. Based on the piezoelectric response of the substrate, the quantitative determination of the PL intensity change and the lateral strain of the BCTZ:Pr film can be obtained. Our results offer an exciting opportunity to realize electrically controlled nonvolatile modulation of lattice-related PL response in ferroelectric oxide heterostructures and design reconfigurable, low-power nonvolatile luminescent memory devices.

Acknowledgments

(PolyU 152753/16E).

References

[1]   X.J. Xie, X.G. Liu, Nat. Mater. 11 (2012) 842.

[2]   D. Chen, Y. Wang, M. Hong, Nano Energy 1 (2012) 73.

[3]   C. Yan, H. Zhao, D.F. Perepichka, F. Rosei, Small 12 (2016) 3888.

[4]   D.K. Khatua, A.Kalaskar, R. Ranjan, Phys. Rev. Lett. 116 (2016) 117601.

[5]   Y. Chen, Y. Zhang, D. Karnaushenko, L. Chen, J. Hao, F. Ding, O.G. Schmidt, Adv. Mater. 29 (2017)1605165.

[6]   L. Chen, M.C. Wong, G. Bai, W. Jie, J. Hao, Nano Energy 14 (2015) 372.

[7]   Y.X. Liu, D.S. Wang, J.X. Shi, Q. Peng, Y.D. Li, Angew. Chem., Int. Ed. 52 (2013) 4366.

[8]   J.H. Hao, Y.Zhang, X.H. Wei, Angew. Chem., Int. Ed. 50 (2011) 6876.

[9]   H.L. Sun, X. Wu, T.H. Chung, K.W. Kwok, Sci. Rep. 6 (2016) 28677.

[10]   H.L. Sun, X. Wu, D.F. Peng, K.W. Kwok, ACS Appl. Mater. Interfaces 9 (2017) 34042.

[11]   G.X. Bai, Y. Zhang, J. Hao, Sci. Rep. 4 (2014) 5724.

[12]   Z.P. Wu, Y. Zhang, G.X. Bai, W.H. Tang, J. Gao, J. Hao, Opt. Express 22 (2014) 29014.

[13]   F.F. Wang, D. Liu, Z.B. Chen, Z.H. Duan, Y. Zhang, D.Z. Sun, X.Y. Zhao, W.Z. Shi, R.K. Zheng, H.S. Luo, J. Mater. Chem. C 5 (2017) 9115.

[14]   T. Wu, P. Zhao, M. Bao, A. Bur, J.L. Hockel, K. Wong, K.P. Mohanchandra, C.S. Lynch, G.P. Carman, J. Appl. Phys. 109 (2011) 124101.

[15]   T. Wu, A. Bur, P. Zhao, K.P. Mohanchandra, K. Wong, K.L. Wang, C.S. Lynch, G.P. Carman, Appl. Phys. Lett. 98 (2011) 012504.

[16]   S. Zhang, Y.G. Zhao, P.S. Li, J.J. Yang, S. Rizwan, J.X. Zhang, J. Seidel, T.L. Qu, Y.J. Yang, Z.L. Luo, Q. He, T. Zou, Q.P. Chen, J.W. Wang, L.F. Yang, Y. Sun, Y.Z. Wu, X. Xiao, X.F. Jin, J. Huang, C. Gao, X.F. Han, R. Ramesh, Phys. Rev. Lett. 108 (2012) 137203.

[17]   Y. Lee, Z.Q. Liu, J.T. Heron, J.D. Clarkson, J. Hong, C. Ko, M.D. Biegalski, U. Aschauer, S.L. Hsu, M.E. Nowakowski, J. Wu, H.M. Christen, S. Salahuddin, J.B. Bokor, N.A. Spaldin, D.G. Schlom, R. Ramesh, Nat. Commun. 6 (2015) 5959.

[18] M. Liu, B.M. Howe, L. Grazulis, K. Mahalingam, T.X. Nan, N.X. Sun, G.J. Brown, Adv. Mater. 25 (2013) 4886.

[19] M. Liu, J. Hoffman, J. Wang, J.X. Zhang, B. Nelson-Cheeseman, A. Bhattacharya, Sci. Rep. 3 (2013)1867.

[20] B.W. Zhi, G.Y. Gao, H.R. Xu, F. Chen, X.L. Tan, P.F. Chen, L.F. Wang, W.B. Wu, ACS Appl. Mater. Interfaces 6 (2014) 4603.

[21] M. Zheng, H. Ni, Y.P. Qi, W.Y. Huang, J.L. Zeng, J. Gao, Appl. Phys. Lett. 110 (2017) 182403.

[22] M. Zheng, Q.X. Zhu, X.Y. Li, M.M. Yang, Y. Wang, X.M. Li, X. Shi, H.S. Luo, R.K. Zheng, J. Appl. Phys. 116 (2014) 113911.

[23] M. Zheng, M.M. Yang, Q.X. Zhu, X.Y. Li, G.Y. Gao, R.K. Zheng, Y. Wang, X.M. Li, X. Shi, H.S. Luo, X.G. Li, Phys. Rev. B 90 (2014) 224420.

[24] M. Zheng, R.K. Zheng, Phys. Rev. Applied 5 (2016) 044002.

[25] M. Zheng, H. Ni, X.K. Xu, Y.P. Qi, X.M. Li, J. Gao, Phys. Rev. Applied 9 (2018) 044039.

[26] W. Liu, X. Ren, Phys. Rev. Lett. 103 (2009) 257602.

[27] P. Zhang, M. Shen, L. Fang, F. Zheng, X. Wu, J. Shen, H. Chen, Appl. Phys. Lett. 92 (2008) 222908.

[28] Q. Zhang, H. Sun, X. Wang, Y. Zhang, X. Li, J. Eur. Ceram. Soc. 34 (2014) 1439.

[29] Y. Huang, L. Luo, J. Wang, Q. Zuo, Y. Yao, W. Li, J. Appl. Phys. 118 (2015) 044101.

[30] B. R. Judd, Phys. Rev. 127 (1962) 750.

[31] G. S. Ofelt, J. Chem. Phys. 37 (1962) 511.

[32] F. Wang, X. Liu, Chem. Soc. Rev. 38 (2009) 976.

[33] X. Wu, C.M. Lau, K.W. Kwok, R.J. Xie, J. Am. Ceram. Soc. 98 (2015) 2139.

[34] M. Zheng, X.K. Xu, H. Ni, Y.P. Qi, X.M. Li, J. Gao, Appl. Phys. Lett. 112 (2018) 123502.

[35] J. Choi, S. Park, J. Lee, K. Hong, D.H. Kim, C.W. Moon, G.D. Park, J. Suh, J. Hwang, S.Y. Kim, H.S. Jung, N.G. Park, S. Han, K.T. Nam, H.W. Jang, Adv. Mater. 28 (2016) 6562-6567.

[36] G. Zhou, S. Duan, P. Li, B. Sun, B. Wu, Y. Yao, X. Yang, J. Han, J. Wu, G. Wang, L.

Liao, C. Lin, W. Hu, C. Xu, D. Liu, T. Chen, L. Chen, A. Zhou, Q. Song, Adv. Electron. Mater. 4 (2018) 1700567.

[37] M. Zheng, H. Ni, W.Y. Huang, Y.P. Qi, J.L. Zeng, J. Gao, Appl. Phys. Lett. 111 (2017) 172901.

[38] S.P. Timoshenko, J.N. Goodier, *Theory of Elasticity* (McGraw-Hill, New York, 1987), Chap. 2.

[39] Y. Wei, Z. Wu, Y. Jia, J. Wu, Y. Shen, H. Luo, Appl. Phys. Lett. 105 (2014) 042902.

[40] H. K. D. Kim, L.T. Schelhas, S. Keller, J.L. Hockel, S.H. Tolbert, G.P. Carman, Nano Lett. 13 (2013) 884.

[41] M. Buzzi, R.V. Chopdekar, J.L. Hockel, A. Bur, T. Wu, N. Pilet, P. Warnicke, G.P. Carman, L.J. Heyderman, F. Nolting, Phys. Rev. Lett. 111 (2013) 027204.

[42] S. Finizio, M. Foerster, M. Buzzi, B. Krüger, M. Jourdan, C.A.F. Vaz, J. Hockel, T. Miyawaki, Tkach, S. Valencia, F. Kronast, G.P. Carman, F. Nolting, M. Kläui, Phys. Rev. Applied 1 (2014) 021001.
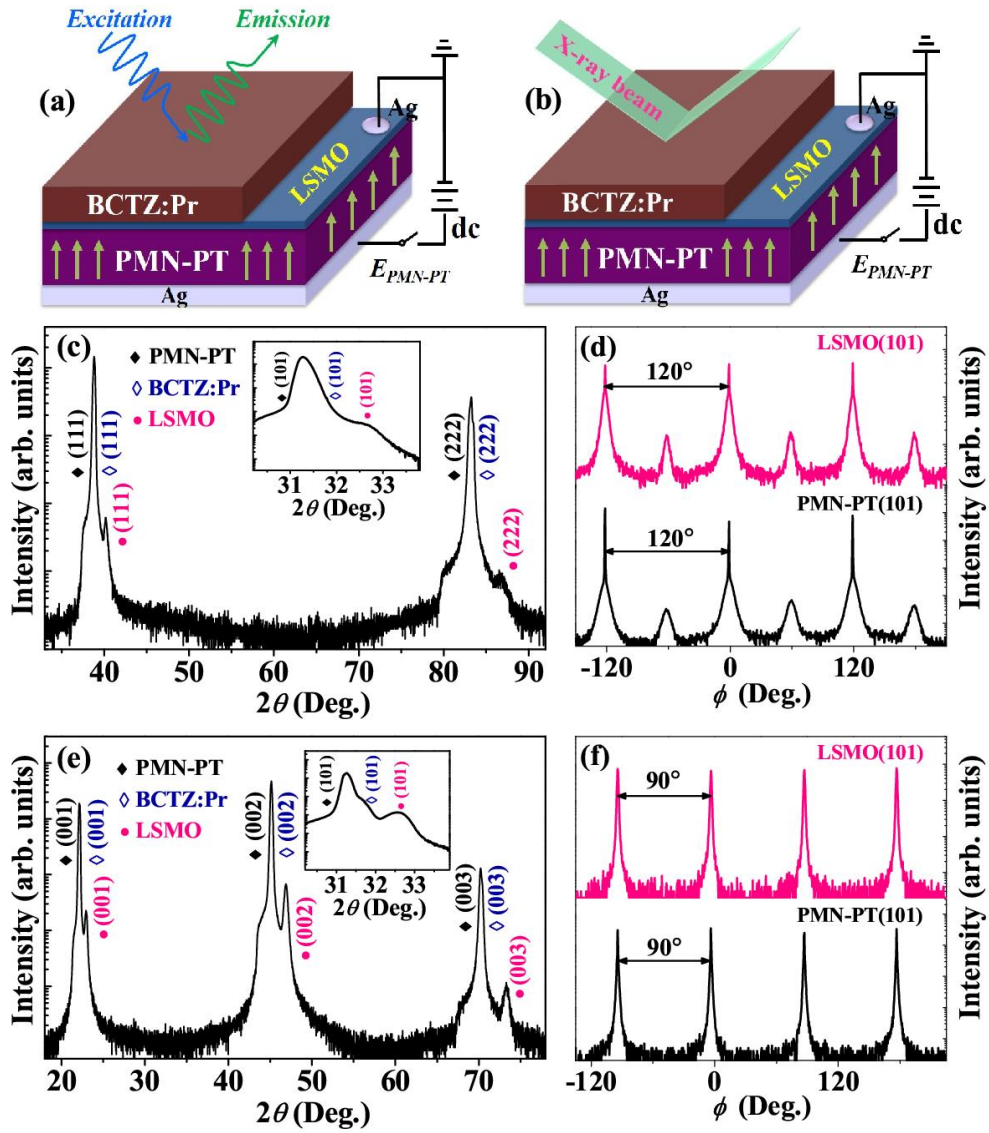
Fig. 1 The electric field configuration for measuring (a) PL response and (b) longitudinal strain of the structure, respectively. (c) and (e) show linear XRD θ-2θ scans of (111)- and (001)-cut BCTZ:Pr/LSMO/PMN-PT heterostructures, respectively. Insets: corresponding off-axis θ-2θ scan data. (d) and (f) XRD ϕ scans of the LSMO (101) and PMN-PT (101) reflection peaks.
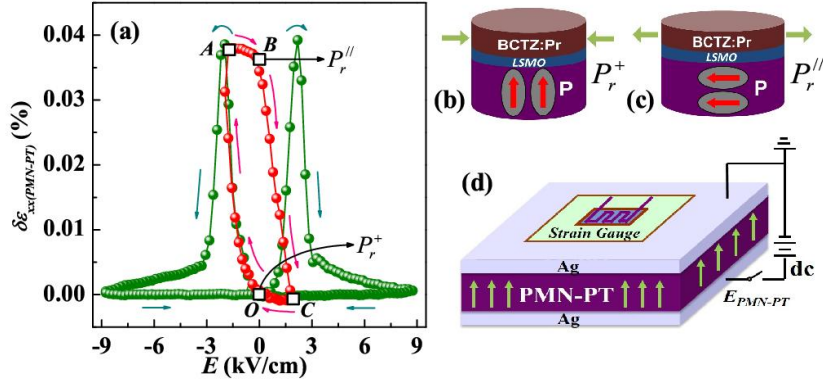
Fig. 2 (a) Electrically induced lateral strain in the PMN-PT(111) under different sweeping fields. The green line and red line are for the amplitude of sweeping field larger and smaller than $E_{C(PMN-PT)}$, respectively. (b) and (c) Schematic illustrations for two ferroelastic strain states. (d) The electric field configuration for measuring lateral strain of the PMN-PT.
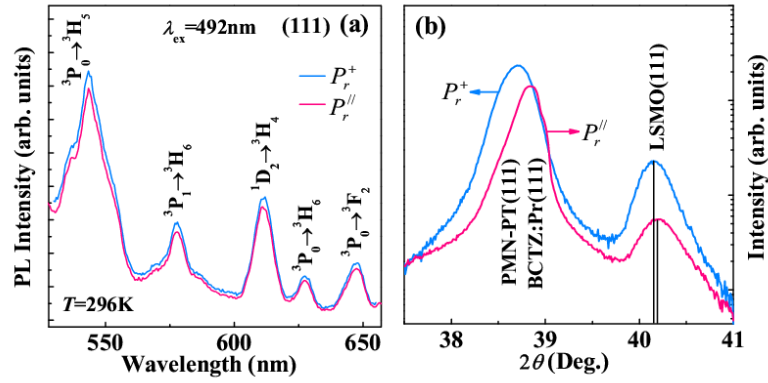
Fig. 3 (a) The PL emission spectra and (b) XRD θ-2θ scans of the BCTZ:Pr/LSMO/PMN-PT(111) heterostructure under the P_r^{+} and $P_r^{//}$ states, respectively.
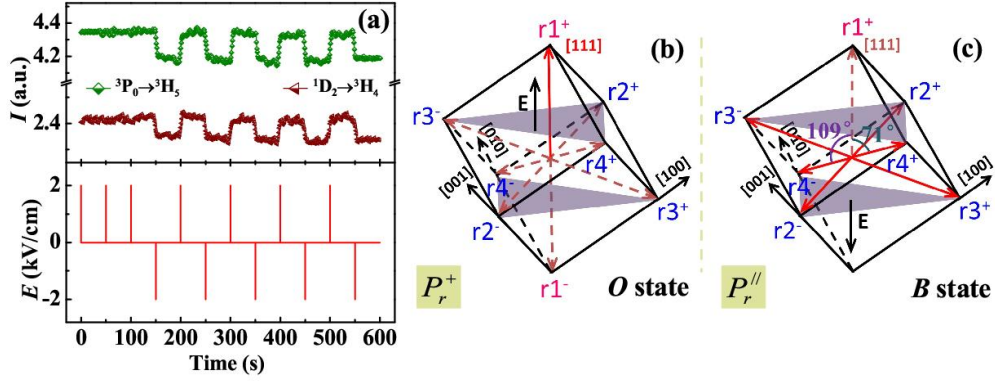
Fig. 4 (a) Nonvolatile PL tuning of the structure by imposing pulse electric fields. (b) and (c) Schematic illustrations for different polarization states (P_r^{+} and $P_r^{//}$) of the PMN-PT.
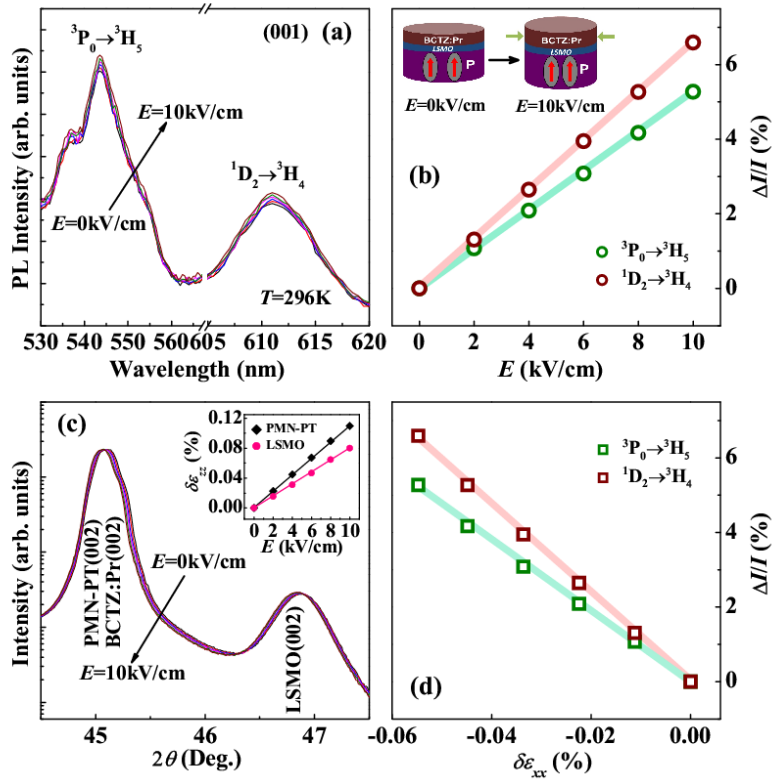
Fig. 5 (a) The PL emission spectra, (b) relative change of PL intensity ($\Delta I/I$), and (c) XRD θ-2θ scans of the BCTZ:Pr/LSMO/PMN-PT(001) structure as a function of positive electric field, respectively. Inset in (b) shows schematic illustrations for converse piezoelectric effect. Inset in (c) shows the electrically induced longitudinal strain $\delta\varepsilon_{zz}$ of the structure. (d) $\Delta I/I$ of the BCTZ:Pr was plotted against lateral strain $\delta\varepsilon_{xx}$ of the PMN-PT.
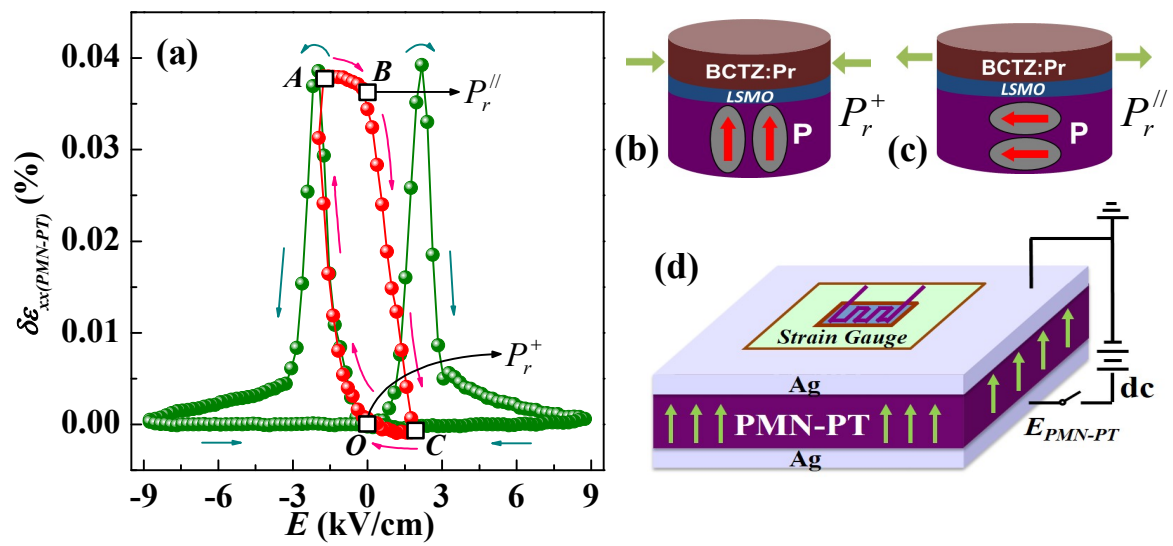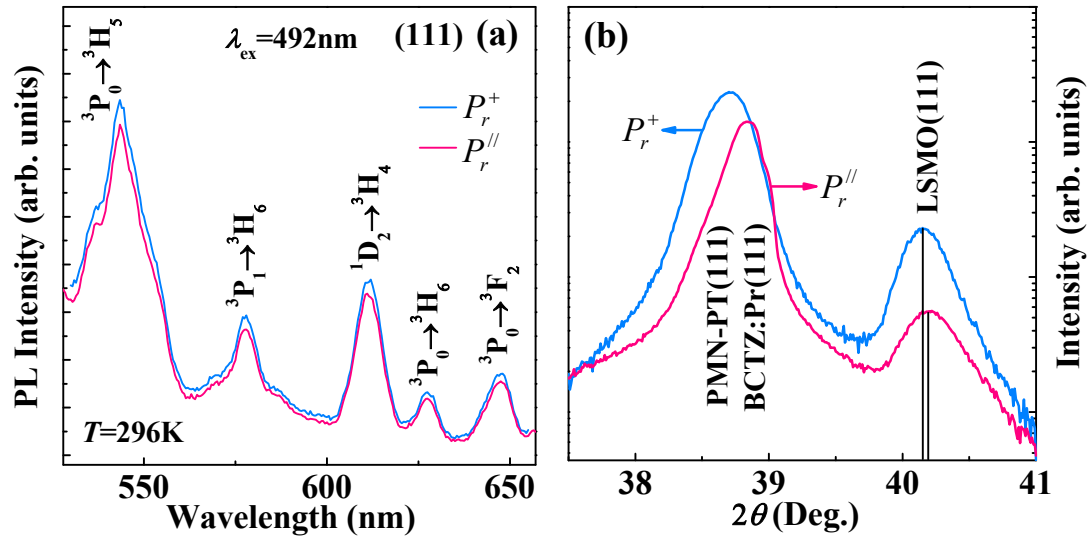
Figure1

Figure 1 by M. Zheng *et al.*
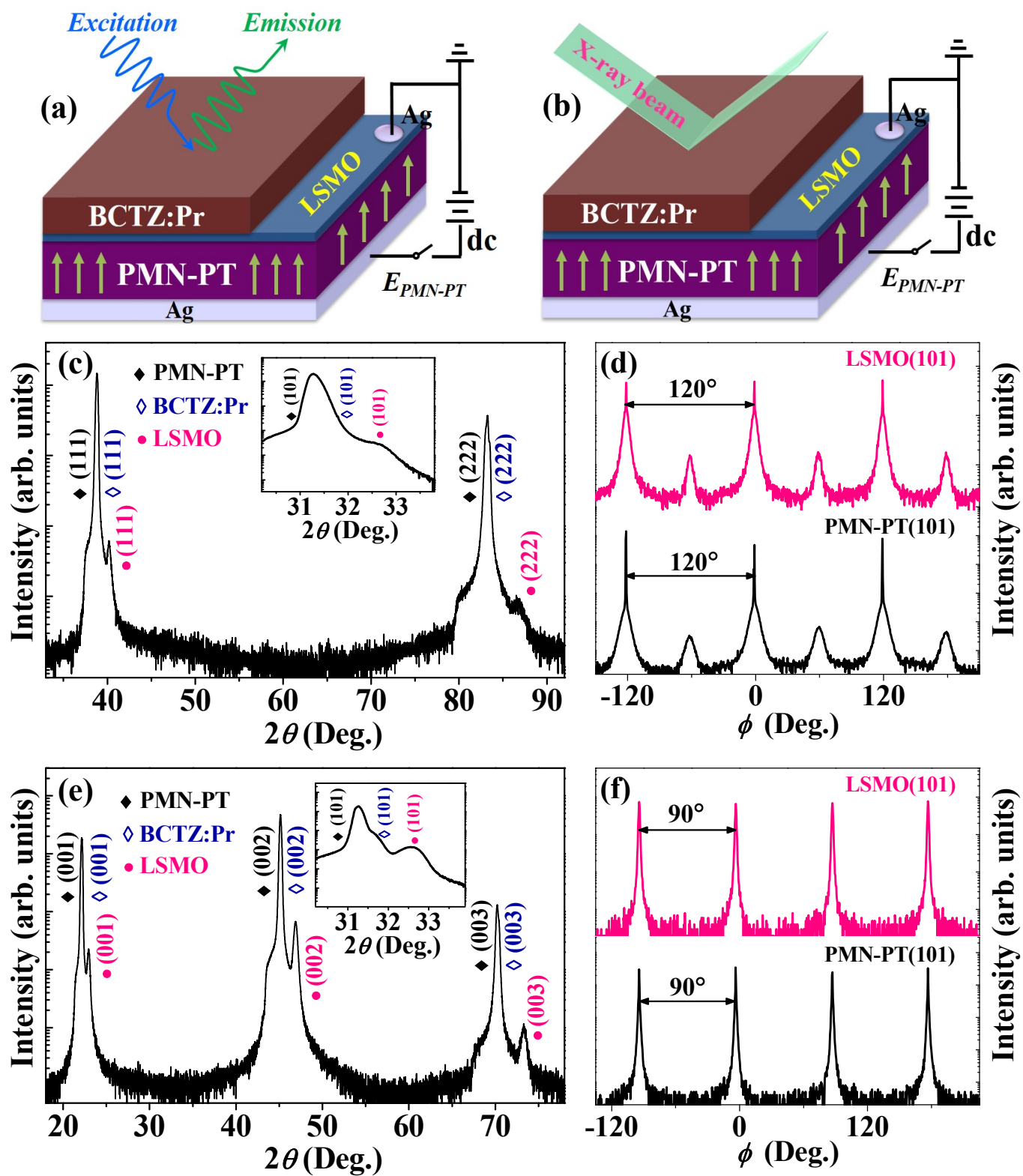
Figure2

Figure 2 by M. Zheng *et al.*

Figure3

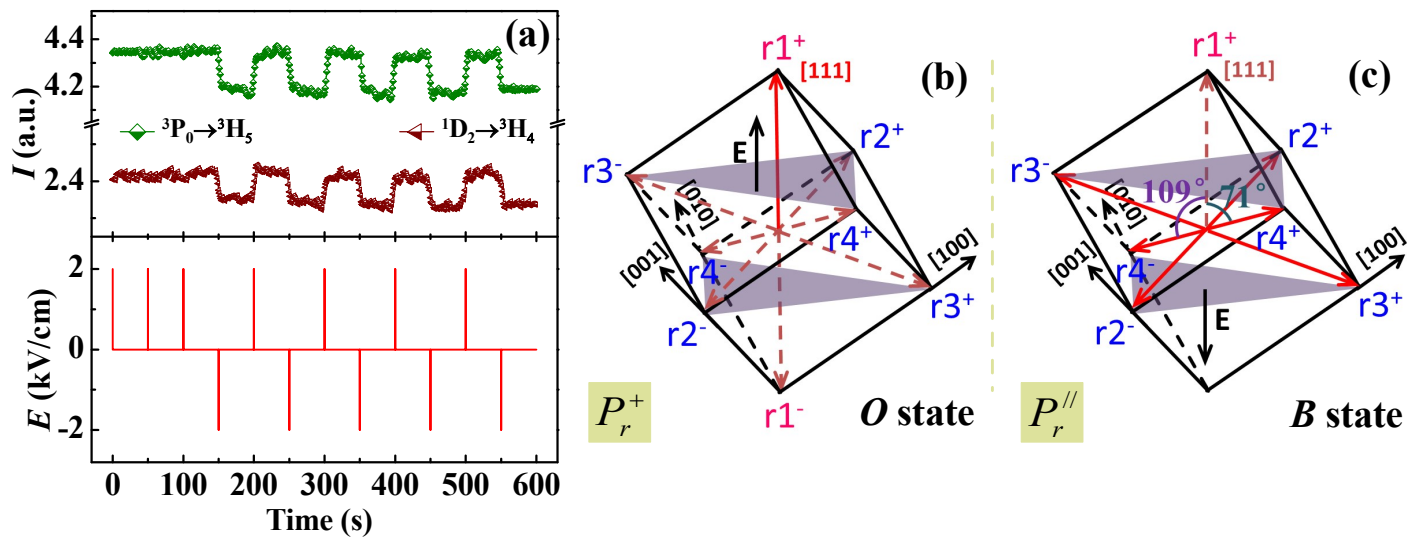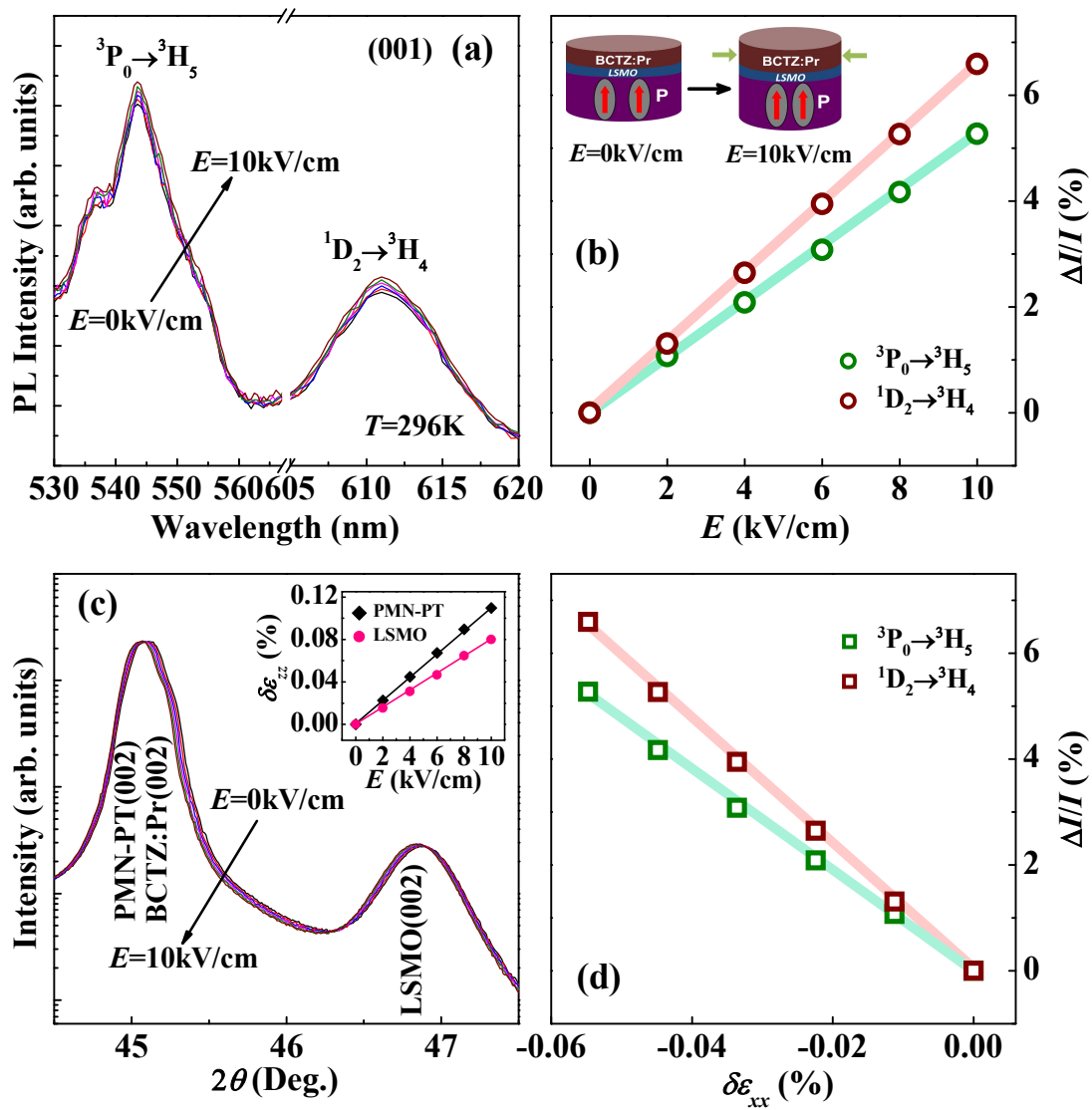# Figure 3 by M. Zheng *et al.*

Figure4

Figure 4 by M. Zheng *et al.*

Figure5

Figure 5 by M. Zheng *et al.*

Supporting Information